Editors' Suggestion | Featured in Physics

Floquet Prethermalization with Lifetime Exceeding 90 s in a Bulk Hyperpolarized Solid

William Beatrez,[1] Otto Janes,[1] Amala Akkiraju,[1] Arjun Pillai,[1] Alexander Oddo,[1] Paul Reshetikhin,[1] Emanuel Druga,[1] Maxwell McAllister,[1] Mark Elo,[2] Benjamin Gilbert,[3] Dieter Suter,[4] and Ashok Ajoy[1,5,*]

[1]*Department of Chemistry, University of California, Berkeley, Berkeley, California 94720, USA*
[2]*Tabor Electronics, Inc., Hatasia 9, Nesher 3660301, Israel*
[3]*Energy Geoscience Division, Lawrence Berkeley National Laboratory, Berkeley, California 94720, USA*
[4]*Fakultät Physik, Technische Universität Dortmund, D-44221 Dortmund, Germany*
[5]*Lawrence Berkeley National Laboratory, Chemical Science Division, University of California, Berkeley, Berkeley, California 94720, USA*

(Received 12 May 2021; accepted 9 September 2021; published 20 October 2021)

We report the observation of long-lived Floquet prethermal states in a bulk solid composed of dipolar-coupled ^{13}C nuclei in diamond at room temperature. For precessing nuclear spins prepared in an initial transverse state, we demonstrate pulsed spin-lock Floquet control that prevents their decay over multiple-minute-long periods. We observe Floquet prethermal lifetimes $T_2' \approx 90.9$ s, extended $> 60\,000$-fold over the nuclear free induction decay times. The spins themselves are continuously interrogated for $\sim$10 min, corresponding to the application of $\approx 5.8 \times 10^6$ control pulses. The ^{13}C nuclei are optically hyperpolarized by lattice nitrogen vacancy centers; the combination of hyperpolarization and continuous spin readout yields significant signal-to-noise ratio in the measurements. This allows probing the Floquet thermalization dynamics with unprecedented clarity. We identify four characteristic regimes of the thermalization process, discerning short-time transient processes leading to the prethermal plateau and long-time system heating toward infinite temperature. This Letter points to new opportunities possible via Floquet control in networks of dilute, randomly distributed, low-sensitivity nuclei. In particular, the combination of minutes-long prethermal lifetimes and continuous spin interrogation opens avenues for quantum sensors constructed from hyperpolarized Floquet prethermal nuclei.

DOI: 10.1103/PhysRevLett.127.170603

Introduction.—Systems pulled away from thermal equilibrium can exhibit unusual phenomena nonexistent or difficult to achieve at equilibrium [1]. For instance, periodically driven quantum systems can display long-lived prethermal lifetimes due to the emergence of approximately conserved quantities under the effective time-independent Hamiltonian describing the drive [2–6]. For sufficiently large driving frequencies ω, much higher than the intrinsic energy scales in the system Hamiltonian (hereafter J), these prethermal lifetimes scale exponentially with ω [7–11]. Ultimately, however, the system absorbs energy and "heats up" to a featureless infinite temperature state.

The long-lived prethermal plateau and its stability against perturbations in the drive portends applications for the engineering of quantum states [3,4,12]. Fundamentally, the control afforded by periodically driven systems opens avenues to study nonequilibrium phenomena and explore novel dynamic phases of matter, some of which have no equilibrium counterparts [13,14]. A flurry of theoretical work has recognized Floquet prethermalization under random driving [15], in driven linear chains [10], and even in the classical limit [16]. Experimentally, Floquet prethermalization has been observed recently in cold-atom [17–19] and NMR systems [20–22]. They demonstrated a characteristic exponential suppression of heating rates with Floquet driving. Even before the current resurgence of interest, decades-old NMR experiments had observed certain signatures of prethermalization, then referred to as "quasi-equilibrium" [23–28].

In this Letter, we report observation of Floquet prethermal states with lifetimes exceeding 90 s at room temperature in a dipolar-coupled ensemble of ^{13}C nuclei in diamond [see Fig. 1(a)]. These nuclear spins, randomly positioned at 1% concentration in the lattice, are optically hyperpolarized by interactions with nitrogen vacancy (NV) defect centers, which enhances their polarization $\varepsilon = 223$-fold with respect to the thermal limit [Fig. 1(b)]. When placed in a Bloch transverse state $\hat{\mathbf{x}}$ in the absence of periodic driving, these precessing nuclei naturally dephase with free induction decay lifetime $T_2^* \approx 1.5$ ms and measured observables decay to zero. Under rapid pulsed spin-lock driving, however, we are able to effect a significant improvement; the observed lifetimes $T_2' \approx 90.9$ s constitute a $> 60\,000$-fold extension over T_2^*. Moreover, with a drive consisting of $\approx 5.8 \times 10^6$ pulses, we are able to continuously probe the thermalization process for up to 573 s with high fidelity. This corresponds to $> 10^{10}$ precession cycles of the nuclear spins. Both with respect to the number of pulses applied, and the ultimate

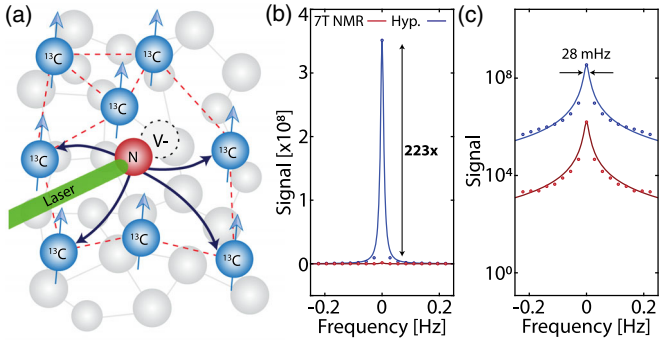

FIG. 1. System. (a) Dipolar lattice of ^{13}C nuclei in diamond. Optically pumped NV centers are employed to hyperpolarize the ^{13}C nuclei (blue arrows). (b),(c) Signal gains from hyperpolarization, demonstrated by comparing single-shot ^{13}C NMR spectra to conventional 7 T (thermal) NMR. Data are shown in (b) linear and (c) log scales; line is a fit. Here, optical pumping was for 2 min at 36 mT, and thermal measurement was taken after 4 hr in the magnet.

transverse spin lifetimes, these values are among the largest reported in literature [29,30]. Our Letter therefore suggests interesting opportunities for Floquet control afforded in hyperpolarizable spin networks consisting of dilute low gyromagnetic ratio nuclei [31].

A primary contribution in this work is the ability to probe the system thermalization dynamics with unprecedented signal-to-noise ratio (SNR). Integrated SNR [see Figs. 1(b) and 1(c)] exceeds 10^8 per shot, including $> 10^3$ per data point (for nearly all $\approx 5.8 \times 10^6$ points), arising from a combination of hyperpolarization and continuous spin readout in our experiments. When $\theta \approx \pi/2$, this amounts to $> 1.4 \times 10^6$ Floquet cycles. This permits a view into the thermalization process with a high degree of clarity, in a manner not directly accessible in previous experiments. Not only does our experiment allow high-SNR continuous-readout access to very large numbers of Floquet cycles, but also offers the ability to discern dynamics within individual cycles. This is an important distinction from simple Magnus expansion treatments, which only give information on stroboscopic dynamics.

We are able to identify the four smoothly transitioning thermalization regimes that confirm theoretical predictions [32]—an initial transient to the prethermal plateau, the crossover to unconstrained thermalization, and, ultimately, infinite temperature. High-SNR measurement also allows characterization of heating rates over a wide range of drive frequencies. We observe system heating scaling $\propto \exp(-t^{1/2})$ at high drive frequency ω. Simultaneously, the transient system response unveils interesting harmonic behavior while establishing the prethermal plateau.

System.—In a magnetic field $\mathbf{B}_0$, the ^{13}C nuclei interact by the dipolar Hamiltonian, $\mathcal{H}_{dd} = \sum_{j<k} d_{jk}^{CC}(3I_{jz}I_{kz} - \vec{I}_j \cdot \vec{I}_k)$, with a coupling strength $d_{jk}^{CC} = (\mu_0/4\pi)\hbar\gamma_n^2 \times (3\cos^2\beta_{jk} - 1)(1/r_{jk}^3)$, where I refer to spin-1/2 Pauli matrices, $\gamma_n = 10.7\,\mathrm{MHz/T}$ is the gyromagnetic ratio, and $\beta_{jk} = \cos^{-1}[(\mathbf{r}_{jk} \cdot \mathbf{B}_0)/r_{jk}B_0]$ is the angle of the internuclear vector $\mathbf{r}_{jk}$ to the magnetic field. The sample is oriented with $\mathbf{B}_0 \| [100]$, such that nearest neighbor ^{13}C sites are decoupled. Ultimately, the median dipolar coupling is $J = \langle d_{jk}^{CC} \rangle \approx 0.66$ kHz [Fig. 2(a)]. The random ^{13}C distribution leads to a long tailed distribution in the coupling values, effectively rendering the interaction Hamiltonian disordered. In addition, the nuclei are subject to on-site disorder, i.e., local dephasing fields, $\mathcal{H}_z = \sum_j c_j I_{jz}$, arising from interactions with paramagnetic impurities (e.g., $P1$ centers) [33]. At typical 20 ppm $P1$ concentrations, $\langle c_j^2 \rangle \approx 0.4\ (\mathrm{kHz})^2$ [34]. In the rotating frame of the Floquet drive, the ^{13}C Hamiltonian is therefore $\mathcal{H} = \mathcal{H}_{dd} + \mathcal{H}_z$.

Compared to previous NMR experiments, our Letter introduces some special features leveraging nuclear hyperpolarization [25,26]. The vast preponderance of NMR experiments have been limited to high-γ_n and dense (100% abundant) nuclei such as ^{19}F, ^{31}P, and ^{1}H [20,22]. Instead, we focus attention to dilute networks of insensitive nuclei (^{13}C). This provides a combination of factors critical to establishing Floquet control for long periods—(i) a relatively low $\|\mathcal{H}_{dd}\|$ compared to networks constructed from sensitive (high-γ_n) nuclei, scaling as $\eta^{1/2}\gamma_n^2$, where η is the nuclear enrichment, (ii) a long tailed distribution in couplings, and (iii) long nuclear T_1 (here $\approx$25 min), significantly higher than many experimental systems, sets a long memory time for the nuclear states.

Indeed, these very factors, while attractive for Floquet control [30], usually make experiments challenging on account of poor sensitivity. Inductively measured nuclear signals scale $\propto \gamma_n^2$, with a measurement repetition rate set by T_1^{-1}, making obtaining reasonable SNR a challenge 35]]. We mitigate these difficulties by a combination of hyperpolarization and instrumental advances (allowing continuous sampling). Hyperpolarization is carried out at $B_{\mathrm{pol}} = 36$ mT through a method previously described [36,37]. Measurement throughput is accelerated by $\approx \frac{1}{2}\epsilon^2[T_1(B_0)/T_1(B_{\mathrm{pol}})]^2(T_2'/T_2^*) \gtrsim 10^{10}$ over conventional high-field (FID-based) NMR readout.

Floquet control and measurement.—The driving protocol is described in Fig. 2(b) [38–40]. After polarization, the ^{13}C nuclei are rotated to transverse axis $\hat{\mathbf{x}}$ on the Bloch sphere, placing them in an initial state $\rho_I \sim \epsilon I_x$. The Floquet drive consists of an equally spaced train of pulses of flip angle θ. The center-to-center pulse separation is $\tau [= (\omega/2\pi)^{-1}]$. After N pulses, the unitary operator describing its action in the rotating frame can be written as $U(N\tau) = [\exp(i\theta I_x)\exp(i\mathcal{H}\tau)]^N$, where we have made a simplifying assumption of δ pulses. The data are sampled after every pulse, $t_j = j\tau$, and the evolution can be described by the operation $U(t) = \prod_{j=1}^{N} \exp(i\mathcal{H}^{(j)}\tau)$, where we refer to the toggling frame Hamiltonians after

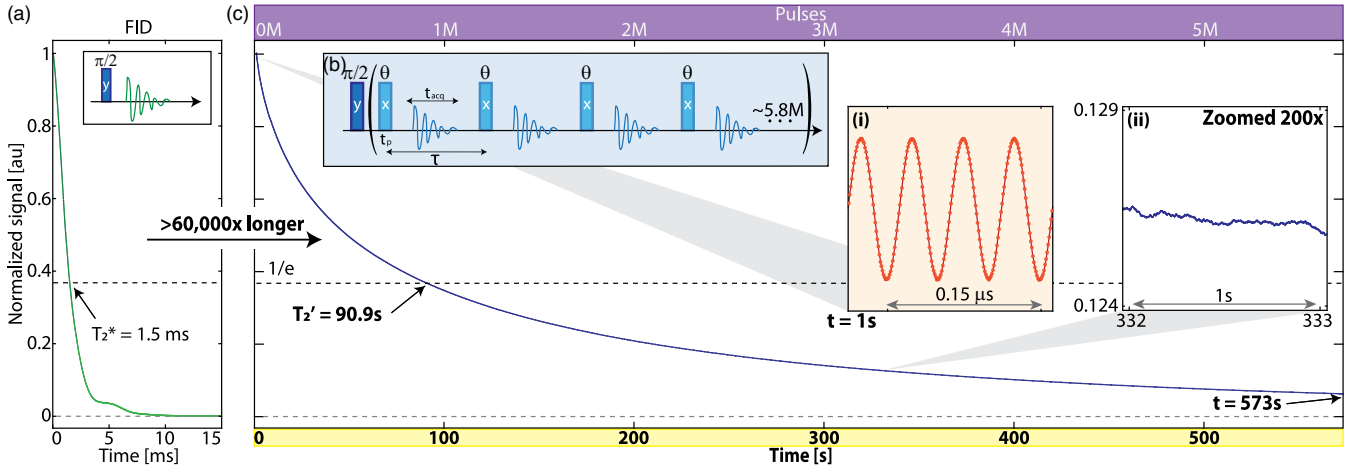

FIG. 2. Floquet driving and lifetime extension. (a) Conventional ^{13}C free induction decay (FID) with $T_2^* \approx 1.5$ ms. (b) Floquet drive consists of a train of θ pulses applied spin-locked with the ^{13}C nuclei. Spins are interrogated in $t_{\rm acq}$ windows between the pulses (blue lines), the nuclear precession is sampled every 1 ns. Pulse repetition rate $\omega = \tau^{-1}$, and sequence not drawn to scale. (c) Minutes-long lifetimes of the transverse state result from the Floquet sequence ($\theta \approx \pi/2$). Data (blue points) shows single-shot measurement of survival probability in the state ρ_I. Here $t_{\rm acq} = 2$ μs, $t_p = 40$ μs and $\tau = 99.28$ μs, and the 573 s period corresponds to $\approx 5.8 \times 10^6$ pulses (upper axis). We neglect here the first 100 ms for clarity [see Fig. 3(a)]. Inset I: raw data showing measurement of the ^{13}C spin precession, here at 1 s into the decay. Inset II: data enlarged 200× in a 1 s window. Using a $1/e$ proxy yields $T_2' \approx 90.9$ s. This corresponds to a $>$ 60 000-fold extension compared to the FID.

every pulse [41], $\mathcal{H}^{(j)} = \exp(ij\theta I_x)\mathcal{H}\exp(-ij\theta I_x)$. This evolution can be recast as $U(t) = \exp(i\mathcal{H}_F N\tau)$, where H_F is the Floquet Hamiltonian that captures the system dynamics under the drive. $\mathcal{H}_F$ can be expanded in a Floquet-Magnus expansion [42–44] to leading order in the parameter $\zeta = 2\pi J/\omega$, and in the regime $\zeta \ll 1$ yields a time-independent Hamiltonian

$$\mathcal{H}_F^{(0)} = \sum_{j=1}^{N} \mathcal{H}^{(j)} \approx \sum_{j<k} d_{jk}^{\rm CC}\left(\frac{3}{2}\mathcal{H}_{\rm ff} - \vec{I}_j \cdot \vec{I}_k\right), \qquad (1)$$

with the flip-flop Hamiltonian $\mathcal{H}_{\rm ff} = I_{jz}I_{kz} + I_{jy}I_{ky}$ [45]. The $\mathcal{H}_z$ dephasing fields are filtered out in $\mathcal{H}_F^{(0)}$. For sufficiently small ζ, Eq. (1) holds irrespective of the flip angle θ, except for certain special values ($\theta \approx \pi$, 2π). We note that this constitutes a key difference with respect to conventional dynamical decoupling control [46], wherein the interspin couplings are retained and result in rapid ^{13}C decay [45]. The higher-order terms in the Magnus expansion are progressively smaller, but contribute to long-time system dynamics [43,47]. Importantly, the initial transverse magnetized state ρ_I is a conserved quantity under $\mathcal{H}_F^{(0)}$, since $[\rho_I, \mathcal{H}_F^{(0)}] = 0$. This leads to prethermal lifetimes that depend exponentially on the drive frequency ω. Ultimately, the divergence of the expansion manifests in the system heating to infinite temperature.

Figure 2(c) shows the measured survival probability $F(N\tau)$ of the state ρ_I under the applied Floquet drive. This can be expressed as $F(N\tau) = \frac{1}{2}\mathrm{Tr}\{\rho_I U(N\tau)^\dagger \rho_I U(N\tau)\}$. We have neglected the first 100 ms here for clarity [see Fig. 3(a) for full data]. Data show significant extension in the transverse state lifetimes. Points in Fig. 2(c) are the experimental data, while the line is a fit to a sum of five exponentials [enlarged in Fig. 2(c)(ii)]; the high-measurement SNR is evident in the enlarged data. The product $J\tau$ is a convenient metric to label the Floquet regime of operation, and in these measurements $J\tau = 0.066$. The $\theta \approx \pi/2$ pulses here are applied every $\tau \approx 100$ μs, and the 573 s period encapsulates $\approx 5.8 \times 10^6$ pulses. For comparison, the conventional ^{13}C free induction decay [48] in the absence of Floquet driving is shown in Fig. 2(a), where decay occurs in $T_2^* \approx 1.5$ ms on account of internuclear couplings and static field disorder. High SNR and continuous weak measurement readout allows us to recognize [see Fig. 3(b)] a dynamic change in the decay rate constant along the curve, making it difficult to quantify the decay rate by a single number. The data, especially past 100 ms, are found to fit well to the stretched exponential $\sim \exp[-(t/T_2')^{1/2}]$, from where we extract $T_2' = 66.7$ s. Alternatively, using a $1/e-$ intersection [dashed line in Fig. 2(c)] as a convenient proxy yields $T_2' = 90.9$ s. The extension leads to substantial line narrowing of the ^{13}C NMR spectrum [$\sim$28 mHz in Fig. 1(c)].

The measurement procedure for Fig. 2(c) is detailed in the Supplemental Material [49]. The signal is sampled every 1 ns in $t_{\rm acq}$ windows between the pulses [see Fig. 2(b)]. The maximum memory size, 16 GB, limits detection to 12×10^9 12-bit samples. Even for a $t_{\rm acq} = 2$ μs window as in Fig. 2(c), this currently limits total acquisition period to 10 min. In any case, such continuous readout (akin to weak

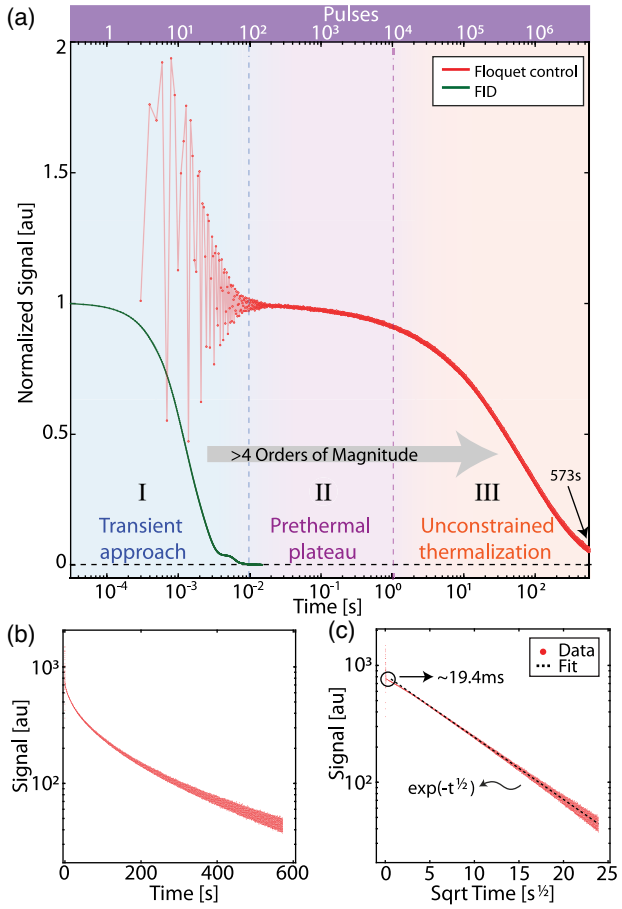

FIG. 3. Floquet thermalization regimes (a) Log-scale visualization of the full data in Fig. 2(c). Points are experiment, there are $\approx 5.8 \times 10^6$ data points here. Upper axis denotes number of pulses applied, here $J\tau \approx 0.066$. Green points are the FID. We observe distinct, yet smoothly transitioning (shaded), thermalization regimes (I–IV): a ≈10 ms oscillatory approach (I) to the Floquet prethermal plateau (II), followed by unconstrained thermalization (III). Infinite temperature regime (IV) is not reached in these measurements up to 573 s. (b) Semilog plot of the experimental data shows a dynamic change of thermalization rate. (c) Semilog plot against $\sqrt{t}$ yields an approximately linear dependence (dashed line) for ∼500 s. Cusp (marked) at ≈ 19.4 ms marks transition to the prethermal plateau (regime II, see also Fig. 5).

measurement [50]) yields significant SNR advantages over point-by-point stroboscopic measurements. Rapid data sampling throughput (at $f_s = \tau^{-1}$) also allows further filtering to be applied when the dynamics are slow compared to f_s. With this, we obtain a single-shot SNR $> 10^3$ per measurement point and $\approx 5 \times 10^8$ for the integrated signal [see Fig. 1(c)].

Floquet prethermalization.—To better illustrate thermalization dynamics of the spins, Fig. 3(a) shows the full data on a logarithmic timescale. The FID is also shown, and lifetime extension is evident from the shift in the curves. Points are experimental data with no moving average applied, and the solid and dashed lines are stretched exponential fits. We identify distinct, albeit smoothly transitioning, regimes in the thermalization process [shaded in Fig. 3(a)]. Following Ref. [2], we refer to them as (I) an initial regime of constrained thermalization ($0 < t <$ 20 ms), where we observe oscillatory behavior with a harmonic frequency response of the Floquet drive frequency ω, (II) the prethermal plateau, leading into (III) unconstrained thermalization toward the (IV) infinite temperature state (not reached in these experiments).

Let us first focus our attention to the dynamics in regimes II and III. Figures 3(b) and 3(c) show two complementary visualizations after moving average filter is applied over the entire data. Figure 3(b), plotted on a semilog scale, makes evident that the decay rate constant changes over the entire thermalization period. The high SNR and rapid sampling rate, however, allows us to unravel the exact rate change behavior in a manner not accessible in previous experiments. It is easiest seen when replotted against $\sqrt{t}$ in Fig. 3(c), where we obtain an approximately linear trend (dashed line) over a long period (∼500 s). The prethermal dynamics is therefore $\sim \exp(-t^{\alpha})$ with exponent $\alpha \approx 1/2$. Decades-old NMR experiments had observed a similar trend in paramagnetic impurity rich solids [51,52]. We emphasize, however, the high SNR of the data in Fig. 3, proffering insights into, and deviations from, this behavior. At higher $J\tau$ values, for instance, we observe a dynamic decrease in α away from $1/2$ in regime III (video available at Ref. [53]). The turning point (cusp) in data in Fig. 3(c), obtained after moving average filtering over the oscillations in regime I, also allows a convenient means to quantify the exact point of transition to prethermal plateau. The length of this period (≈10–20 ms) closely mirrors the period over which the FID completely decays [see Fig. 3(a)].

To study the scaling of the prethermal lifetimes with the frequency of the Floquet drive ω, Fig. 4(a) shows similar data at a range of $J\tau$ values. This is carried out by varying the interpulse spacing τ in Fig. 2(b). The full dataset (shown in the Supplemental Material [49]) consists of measurements at 57 such $J\tau$ values, but we show a restricted set here for clarity. Again, there is a high density of data points in each experimental line. To restrict attention to regions II and III, we normalize the data at the transition points to the prethermal plateau, identified from the cusps as in Fig. 3(c). The data show thermalization proceeding more slowly for lower values of $J\tau$. The dynamic change of rate coefficient makes plotting a single graph that encapsulates the full long-time behavior difficult. Instead, we extract the decay rates focusing on regimes II and III, where decay [similar to Fig. 3(c)] follows an exponent $\alpha \approx 1/2$.

This is presented in two complementary viewpoints in Figs. 4(b) and 4(c). First, in Fig. 4(b) plotted on a semilog scale with respect to the drive period τ, we see a linear trend in the decay rates, especially at high τ (dashed line). This points to an approximately exponential scaling of the state preservation lifetimes with drive frequency, one of the signatures of Floquet prethermalization. At low τ,

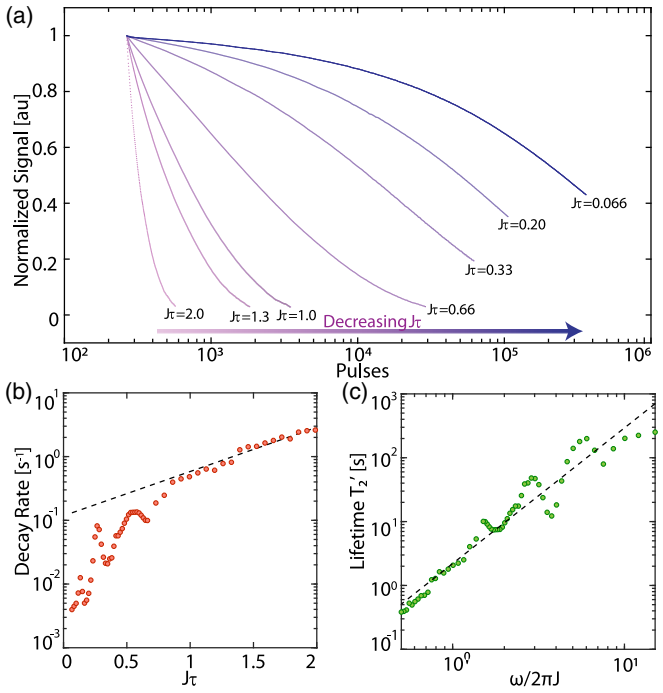

FIG. 4. Exponential dependence of Floquet prethermal lifetimes. (a) Variation with $J\tau$. Data (points) show measured signal probing thermalization dynamics in regimes II and III for representative $J\tau$ values (color bar). Here $\theta \approx \pi/2$ and $t_{\mathrm{acq}} = 32\ \mu$s and there are a high number ($\sim 10^3 - 10^6$) points per line [49]. Data are normalized at the transition points to the prethermal plateau [following Fig. 3(c)]. The Floquet prethermal decay rates reduce considerably with decreasing $J\tau$. See full data at Ref. [53]. (b) Extracted decay rates focusing on the region where decay follows $\sim \exp(-t^{1/2})$. Plotted in a semilog scale against $J\tau$, the dashed line reveals an approximately exponential scaling of the decay rates at high drive periods τ (dashed line is a linear fit). At low τ we observe sharp narrow features in the prethermal decay rates. (c) Log-log plot of the extracted transverse state lifetimes T_2' against ω/J (dashed line is a linear fit).

however, we observe a flatter slope with sharp features in the decay rates. Figure 4(c) shows an alternate view instead in terms of ω. Extracting the transverse state lifetimes T_2' on the log-log plot, we find a slope of 2.1 ± 0.1 at low frequency, suggesting a Fermi's golden rule scaling with drive frequency [54]. Since Rabi frequency is relatively low in our experiments, the lowest $J\tau$ value accessible was 0.066. We estimate that the filling factor of the rf coil employed for ^{13}C readout in our experiments can be improved by about an order of magnitude. The scaling observed in Fig. 4 suggests that such an improvement in $J\tau$ would result in significant gains in T_2' lifetimes.

The sharp peaks in the decay rates in the high-ω regime in Figs. 4(b) and 4(c) are intriguing. We believe this is a manifestation of quantum sensing—the ^{13}C nuclei see an enhanced decay rate when subjected to environmental magnetic fields at a fixed frequency f_{ac} matched in periodicity (resonant) with the pulse sequence, at $f_{\mathrm{ac}} = \theta/(2\pi\tau)$. The first two peaks are observed at $f_{\mathrm{ac}} \approx 2.5$ and $f_{\mathrm{ac}} \approx 5.0$ kHz. This is possible because the pulsed spin-lock sequence exhibits dynamical decoupling properties similar to quantum sensing protocols [31]. The exact origin of these fields in Figs. 4(b) and 4(c) are unclear and beyond the scope of the current Letter. A more detailed exposition on exploiting Floquet prethermal states for quantum sensing will be presented elsewhere.

Approach to prethermal plateau.—Finally, let us elucidate how the nuclear spins approach the Floquet prethermal plateau [55], focusing attention on regime I of Fig. 3(a). We observe transients in the survival probability leading into the plateau; this is shown for two choices of the flip angle θ in Fig. 5(a) ($\theta \approx \pi/2$ and $\theta \approx \pi/4$, respectively). High SNR allows us to track the oscillatory dynamics after every pulse, providing a window into how the approximately time-independent Hamiltonian is established. Moreover, the prethermal plateau level is itself dependent on θ.

The transients last for $t \approx 10$ ms, which is approximately the total lifetime for the original FID, and is of the order of magnitude of $\|\mathcal{H}_{dd}\|^{-1}$ [see Fig. 3(a)]. As Fig. 5(b) indicates, the oscillation periodicity is closely related to the flip angle employed; for $\theta \approx \pi/2$, for instance, the oscillations occur at a fourth of the frequency of the Floquet drive ω. To see this more clearly, Fig. 5(c) shows the respective Fourier transforms in a 10 ms region. Plotted against ω, we identify harmonics of the oscillatory dynamics (numbers). For $\theta \approx \pi/4$ [lower panels in Figs. 5(b) and 5(c)], we recognize a primary harmonic and higher harmonics at $\approx n\omega/8$, where n is an integer.

Intuitively, this characteristic periodicity can be thought of as arising from the number of pulses N_k required to return the Floquet unitary to a prior configuration; i.e., the toggling frame Hamiltonian after $2N_k$ pulses is equivalent to that after N_k, $\mathcal{H}^{(2N_k)} = \mathcal{H}^{(N_k)}$. This corresponds to effectively completing a 2π rotation of the Hamiltonian in the toggling frame. Four pulses are therefore needed for $\theta = \pi/2$ in Fig. 5(a). In general, the primary harmonic frequency is expected to be at frequency $f = \theta/(2\pi\tau)$. Experiments confirm this picture; we extract the oscillation frequencies in regime I as a function of θ, and they fall neatly onto three straight lines for the three harmonics [see Fig. 5(d)]. We hypothesize that the higher harmonics arise from bi- and trilinear terms in the density matrix produced by dipolar evolution. The experimentally measured slopes are in the ratio 1:1.98:2.93, close to the 1:2:3 pattern expected. The precise deviation of these ratios from 1:2:3, as well as the nonzero intercept of the extrapolated fits in Fig. 5(d) are experimental surprises that will be the subject of future work. We note that this question is outside the scope of a Magnus expansion treatment and relates to how an average Hamiltonian is established in the first place.

In conclusion, we have observed Floquet prethermalization of dipolar-coupled nuclear spins in a bulk solid at

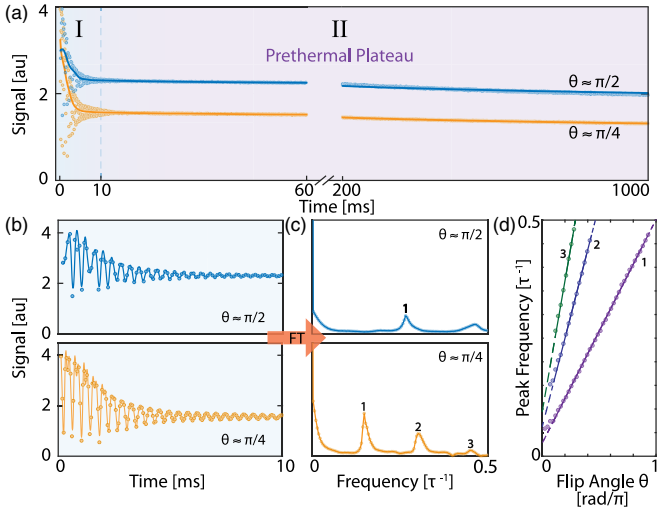

FIG. 5. Transient approach to prethermal plateau. (a) Oscillations in the approach to prethermal plateau seen for data enlarged in region I, in a 1-s-long window [see Fig. 3(a)]. Data (points) correspond to $\theta \approx \{\pi/2, \pi/4\}$, respectively. Solid line is data, with moving average filtering applied over the entire region [see Fig. 3(b)]. (b) Enlarged region I shows the transient approach with high SNR. It is evident that the oscillations are at higher frequency for $\theta \approx \pi/2$. Solid line is a spline fit to guide the eye. (c) Fourier transforms of panels in (b) allows identification of the frequency components constituting the oscillations as a function of $\omega = \tau^{-1}$. Harmonics are represented by numbers. It is clear that primary oscillation frequency is higher for $\theta \approx \pi/2$, where we extract the primary harmonic position at $\approx 0.26\tau^{-1}$. (d) Variation with flip angle θ. Data show the position of the oscillation frequency for the primary and higher harmonics (numbered). See full data at Ref. [56]. Solid lines are linear fits, while dashed line is an extrapolation. Slopes are in the ratio expected.

room temperature. The observed > 90-s-long prethermal lifetimes in diamond ^{13}C nuclei are over 4 orders of magnitude longer than free induction decay times and significantly longer than in other systems. Our measurements unveil regimes of thermalization with a degree of clarity not accessible in previous NMR studies. Apart from fundamental insights, our Letter points to attractive opportunities possible via Floquet control in hyperpolarizable, dilute, and low-γ_n nuclear networks. Protection and continuous interrogation of spins along a Bloch transverse axis for ~10 min periods opens avenues for high-sensitivity magnetometers, gyroscopes [57,58], and spin sensors [59] constructed out of hyperpolarized prethermal ^{13}C nuclei.

We gratefully acknowledge M. Markham (Element6), for the diamond sample used in this work, and discussions with S. Bhave, M. Bukov, C. Fleckenstein, C. Meriles, J. Reimer, D. Sakellariou, and A. Souza. This work was funded by ONR under Contract No. N00014-20-1-2806. B. G. was supported by DOE BES CSGB under Award No. DE-AC02-05CH11231.

*ashokaj@berkeley.edu

[1] L. F. Santos, The quick drive to pseudo-equilibrium, Nat. Phys. **17**, 429 (2021).
[2] L. D'Alessio and M. Rigol, Long-Time Behavior of Isolated Periodically Driven Interacting Lattice Systems, Phys. Rev. X **4**, 041048 (2014).
[3] N. Goldman and J. Dalibard, Periodically Driven Quantum Systems: Effective Hamiltonians and Engineered Gauge Fields, Phys. Rev. X **4**, 031027 (2014).
[4] M. Bukov, L. D'Alessio, and A. Polkovnikov, Universal high-frequency behavior of periodically driven systems: From dynamical stabilization to Floquet engineering, Adv. Phys. **64**, 139 (2015).
[5] D. A. Abanin, W. De Roeck, and F. Huveneers, Exponentially Slow Heating in Periodically Driven Many-Body Systems, Phys. Rev. Lett. **115**, 256803 (2015).
[6] A. Lazarides, A. Das, and R. Moessner, Equilibrium states of generic quantum systems subject to periodic driving, Phys. Rev. E **90**, 012110 (2014).
[7] T. Kuwahara, T. Mori, and K. Saito, Floquet–magnus theory and generic transient dynamics in periodically driven many-body quantum systems, Ann. Phys. (Amsterdam) **367**, 96 (2016).
[8] M. Bukov, S. Gopalakrishnan, M. Knap, and E. Demler, Prethermal Floquet Steady States and Instabilities in the Periodically Driven, Weakly Interacting Bose-Hubbard Model, Phys. Rev. Lett. **115**, 205301 (2015).
[9] D. A. Abanin, W. De Roeck, W. W. Ho, and F. Huveneers, Effective Hamiltonians, prethermalization, and slow energy absorption in periodically driven many-body systems, Phys. Rev. B **95**, 014112 (2017).
[10] S. A. Weidinger and M. Knap, Floquet prethermalization and regimes of heating in a periodically driven, interacting quantum system, Sci. Rep. **7**, 45382 (2017).
[11] D. J. Luitz, R. Moessner, S. L. Sondhi, and V. Khemani, Prethermalization without Temperature, Phys. Rev. X **10**, 021046 (2020).
[12] K. Singh, C. J. Fujiwara, Z. A. Geiger, E. Q. Simmons, M. Lipatov, A. Cao, P. Dotti, S. V. Rajagopal, R. Senaratne, T. Shimasaki, M. Heyl, A. Eckardt, and D. M. Weld, Quantifying and Controlling Prethermal Nonergodicity in Interacting Floquet Matter, Phys. Rev. X **9**, 041021 (2019).
[13] D. V. Else and C. Nayak, Classification of topological phases in periodically driven interacting systems, Phys. Rev. B **93**, 201103(R) (2016).
[14] V. Khemani, A. Lazarides, R. Moessner, and S. L. Sondhi, Phase Structure of Driven Quantum Systems, Phys. Rev. Lett. **116**, 250401 (2016).
[15] H. Zhao, F. Mintert, R. Moessner, and J. Knolle, Random Multipolar Driving: Tunably Slow Heating through Spectral Engineering, Phys. Rev. Lett. **126**, 040601 (2021).
[16] O. Howell, P. Weinberg, D. Sels, A. Polkovnikov, and M. Bukov, Asymptotic Prethermalization in Periodically Driven Classical Spin Chains, Phys. Rev. Lett. **122**, 010602 (2019).
[17] A. Rubio-Abadal, M. Ippoliti, S. Hollerith, D. Wei, J. Rui, S. L. Sondhi, V. Khemani, C. Gross, and I. Bloch, Floquet Prethermalization in a Bose-Hubbard System, Phys. Rev. X **10**, 021044 (2020).

[18] K. Viebahn, J. Minguzzi, K. Sandholzer, A.-S. Walter, M. Sajnani, F. Görg, and T. Esslinger, Suppressing Dissipation in a Floquet-Hubbard System, Phys. Rev. X **11**, 011057 (2021).
[19] M. Ueda, Quantum equilibration, thermalization and prethermalization in ultracold atoms, Nat. Rev. Phys. **2**, 669 (2020).
[20] P. Peng, C. Yin, X. Huang, C. Ramanathan, and P. Cappellaro, Floquet prethermalization in dipolar spin chains, Nat. Phys. **17**, 444 (2021).
[21] C. Yin, P. Peng, X. Huang, C. Ramanathan, and P. Cappellaro, Prethermal quasiconserved observables in Floquet quantum systems, Phys. Rev. B **103**, 054305 (2021).
[22] J. Rovny, R. L. Blum, and S. E. Barrett, Observation of Discrete-Time-Crystal Signatures in an Ordered Dipolar Many-Body System, Phys. Rev. Lett. **120**, 180603 (2018).
[23] M. M. Maricq, Spin thermodynamics of periodically time-dependent systems: The quasistationary state and its decay, Phys. Rev. B **36**, 516 (1987).
[24] M. M. Maricq, Long-time limitations of the average Hamiltonian theory: A dressed-states viewpoint, in *Advances in Magnetic Resonance: The Waugh Symposium* (Academic Press, New York, 1990), pp. 151–182.
[25] D. Sakellariou, P. Hodgkinson, and L. Emsley, Quasi equilibria in solid-state NMR, Chem. Phys. Lett. **293**, 110 (1998).
[26] D. Sakellariou, P. Hodgkinson, S. Hediger, and L. Emsley, Experimental observation of periodic quasi-equilibria in solid-state NMR, Chem. Phys. Lett. **308**, 381 (1999).
[27] J. b. Waugh, Equilibrium and ergodicity in small spin systems, Mol. Phys. **95**, 731 (1998).
[28] R. Bruschweiler and R. Ernst, Non-ergodic quasi-equilibria in short linear spin 12 chains, Chem. Phys. Lett. **264**, 393 (1997).
[29] T. D. Ladd, D. Maryenko, Y. Yamamoto, E. Abe, and K. M. Itoh, Coherence time of decoupled nuclear spins in silicon, Phys. Rev. B **71**, 014401 (2005).
[30] Y. Dong, R. G. Ramos, D. Li, and S. E. Barrett, Controlling Coherence Using the Internal Structure of Hard π Pulses, Phys. Rev. Lett. **100**, 247601 (2008).
[31] C. L. Degen, F. Reinhard, and P. Cappellaro, Quantum sensing, Rev. Mod. Phys. **89**, 035002 (2017).
[32] C. Fleckenstein and M. Bukov, Thermalization and prethermalization in periodically kicked quantum spin chains, Phys. Rev. B **103**, 144307 (2021).
[33] E. Reynhardt and C. Terblanche, 13c relaxation in natural diamond, Chem. Phys. Lett. **269**, 464 (1997).
[34] A. Ajoy, B. Safvati, R. Nazaryan, J. Oon, B. Han, P. Raghavan, R. Nirodi, A. Aguilar, K. Liu, X. Cai *et al.*, Hyperpolarized relaxometry based nuclear t 1 noise spectroscopy in diamond, Nat. Commun. **10**, 5160 (2019).
[35] D. Hoult, The NMR receiver: A description and analysis of design, Prog. Nucl. Magn. Reson. Spectrosc. **12**, 41 (1978).
[36] A. Ajoy, K. Liu, R. Nazaryan, X. Lv, P. R. Zangara, B. Safvati, G. Wang, D. Arnold, G. Li, A. Lin *et al.*, Orientation-independent room temperature optical 13c hyperpolarization in powdered diamond, Sci. Adv. **4**, eaar5492 (2018).
[37] A. Ajoy, R. Nazaryan, K. Liu, X. Lv, B. Safvati, G. Wang, E. Druga, J. Reimer, D. Suter, C. Ramanathan *et al.*, Enhanced dynamic nuclear polarization via swept microwave frequency combs, Proc. Natl. Acad. Sci. U.S.A. **115**, 10576 (2018).
[38] E. Ostroff and J. Waugh, Multiple Spin Echoes and Spin Locking in Solids, Phys. Rev. Lett. **16**, 1097 (1966).
[39] W.-K. Rhim, D. Burum, and D. Elleman, Multiple-Pulse Spin Locking in Dipolar Solids, Phys. Rev. Lett. **37**, 1764 (1976).
[40] W.-K. Rhim, D. Burum, and D. Elleman, Calculation of spin-lattice relaxation during pulsed spin locking in solids, J. Chem. Phys. **68**, 692 (1978).
[41] U. Haeberlen, *High Resolution NMR in Solids: Selective Averaging* (Academic Press, Inc., New York, 1976).
[42] W. Magnus, On the exponential solution of differential equations for a linear operator, Commun. Pure Appl. Math. **7**, 649 (1954).
[43] R. M. Wilcox, Exponential operators and parameter differentiation in quantum physics, J. Math. Phys. (N.Y.) **8**, 962 (1967).
[44] S. Blanes, F. Casas, J. Oteo, and J. Ros, The Magnus expansion and some of its applications, Phys. Rep. **470**, 151 (2009).
[45] A. Ajoy, R. Nirodi, A. Sarkar, P. Reshetikhin, E. Druga, A. Akkiraju, M. McAllister, G. Maineri, S. Le, A. Lin *et al.*, Dynamical decoupling in interacting systems: Applications to signal-enhanced hyperpolarized readout, arXiv:2008.08323.
[46] H. Y. Carr and E. M. Purcell, Effects of diffusion on free precession in nuclear magnetic resonance experiments, Phys. Rev. **94**, 630 (1954).
[47] R. Ernst, G. Bodenhausen, and A. Wokaun, *Principles of Nuclear Magnetic Resonance in One and Two Dimensions* (Clarendon Press, Oxford, 1987).
[48] I. Lowe, Free Induction Decays of Rotating Solids, Phys. Rev. Lett. **2**, 285 (1959).
[49] See Supplemental Material at http://link.aps.org/supplemental/10.1103/PhysRevLett.127.170603 for details on experimental measurement and data processing.
[50] M. Pfender, P. Wang, H. Sumiya, S. Onoda, W. Yang, D. B. R. Dasari, P. Neumann, X.-Y. Pan, J. Isoya, R.-B. Liu *et al.*, High-resolution spectroscopy of single nuclear spins via sequential weak measurements, Nat. Commun. **10**, 594 (2019).
[51] D. Tse and S. Hartmann, Nuclear Spin-Lattice Relaxation via Paramagnetic Centers without Spin Diffusion, Phys. Rev. Lett. **21**, 511 (1968).
[52] N.-a. Lin and S. Hartmann, Nuclear spin-lattice relaxation in ca f 2 via paramagnetic centers for short correlation time when spin diffusion is inhibited, Phys. Rev. B **8**, 4079 (1973).
[53] Video showing full dataset of Fig. 4: https://www.youtube.com/watch?v=uLKIR_XM_FQ (2021).
[54] C. Fleckenstein and M. Bukov, Prethermalization and thermalization in periodically driven many-body systems away from the high-frequency limit, Phys. Rev. B **103**, L140302 (2021).
[55] A. Haldar, R. Moessner, and A. Das, Onset of Floquet thermalization, Phys. Rev. B **97**, 245122 (2018).
[56] Video showing full dataset of Fig. 5: https://www.youtube.com/watch?v=8NI7Zzugi4o (2021).

[57] A. Ajoy and P. Cappellaro, Stable three-axis nuclear-spin gyroscope in diamond, Phys. Rev. A **86**, 062104 (2012).
[58] M. P. Ledbetter, K. Jensen, R. Fischer, A. Jarmola, and D. Budker, Gyroscopes based on nitrogen-vacancy centers in diamond, Phys. Rev. A **86**, 052116 (2012).
[59] M. Abobeih, J. Randall, C. Bradley, H. Bartling, M. Bakker, M. Degen, M. Markham, D. Twitchen, and T. Taminiau, Atomic-scale imaging of a 27-nuclear-spin cluster using a quantum sensor, Nature (London) **576**, 411 (2019).